Available online at www.sciencedirect.com
ScienceDirect
Ceramics International 35 (2009) 3043–3049
CERAMICS INTERNATIONAL
www.elsevier.com/locate/ceramint

Surface modification of bovine bone ash prepared by milling and acid washing process

Douglas Gouvêa [a,*], Gerardo A.V. Alatrista [a], Silvio L.M. Brito [a], Ricardo H.R. Castro [b], H. Kahn [c]

[a] *Department of Metallurgical and Materials Engineering, Escola Politécnica, University of São Paulo, Av. Prof. Mello Moraes, 2463 São Paulo, SP 05508-900, Brazil*
[b] *Chemical Engineering and Materials Science Department, UC Davis, Davis, CA 95616, USA*
[c] *Department of Mining and Petroleum Engineering, Escola Politécnica, University of São Paulo, Av. Prof. Mello Moraes, 2373 São Paulo, SP 05508-900, Brazil*

Received 27 November 2008; received in revised form 4 February 2009; accepted 12 April 2009
Available online 6 June 2009

Abstract

Bovine bone ash is the main raw material for fabrication of bone china, a special kind of porcelain that has visual and mechanical advantages when compared to usual porcelains. The properties of bone china are highly dependent on the characteristics of the bone ash. However, despite a relatively common product, the science behind formulations and accepted fabrication procedures for bone china is not completely understood and deserves attention for future processing optimizations. In this paper, the influence of the preparation steps (firing, milling, and washing of the bones) on the physicochemical properties of bone ash particles was investigated. Bone powders heat-treated at temperatures varying from 700 to 1000 °C were washed and milled. The obtained materials were analyzed in terms of particle size distribution, chemical composition, density, specific surface area, FTIR spectroscopy, dynamic electrophoretic mobility, crystalline phases and scanning electron microscopy. The results indicated that bone ash does not significantly change in terms of chemistry and physical features at calcination temperatures above 700 °C. After washing in special conditions, one could only observe hydroxyapatite in the diffraction pattern. By FTIR it was observed that carbonate seems to be mainly concentrated on the surface of the powders. Since this compound can influence in the dispersion stability, and consequently in the quality of the final bone china product, and considering optimal washing parameters based on the dynamic electrophoretic mobility results, we describe a procedure for surface cleaning.

Keywords: A. Calcination; A. Milling; A. Suspensions; B. Interfaces; D. Porcelain

1. Introduction

Bovine bone ash is the main raw material for the production of bone china. The typical composition of a commercial bone china is 25% (w/w) clay, 25% (w/w) Cornish stone and 50% (w/w) bovine bone ash. This special kind of porcelain has higher mechanical and optical properties when compared to common even with a relatively low sintering temperature (1280 °C) [1]. These properties guarantee a regular market for bone china among china.

The cost of bone in the bone china production was estimated to be around 9.6% [2]. This is a significant part of the total cost and optimization of bone ash production could drive an important reduction of final cost of bone china manufacture [2]. The traditional process of bone ash production comprises a first step where most meat and protein are removed by treatment with hot water, steam or solvents [3]. After that, the bone is dried and heat-treated, usually at 1000 °C, to remove all the remaining organic compounds [3]. Finally, it is milled until a fine white powder is obtained. The final product is basically hydroxyapatite with a chemical formula: $Ca_{10}(PO_4)_6OH_2$. Despite a traditional fabrication procedure of bone china, the times and temperatures of heat treatments to be used are not well justified in the literature, and this can be a source for cost reductions by optimization of the process.

* Corresponding author. Tel.: +55 11 30915238; fax: +55 11 30915421.
E-mail address: dgouvea@usp.br (D. Gouvêa).

0272-8842/$36.00
doi:10.1016/j.ceramint.2009.04.024

A great number of works reports on the chemical reactions and phases transformations occurring during sintering, glaze formation, and glazing of bone china [4–14]. However, less attention has been paid to the study of the effect of variables such as calcination temperature and atmosphere, or washing/milling conditions on the particle size distribution, specific surface area and physical–chemical surface properties of the calcined bovine bone powders [3]. These variables directly affect the microstructure of the bone powders that influences the processing parameters and final characteristics of the product. Recently, hydroxyapatite produced from bone ash brought attention of the prosthesis market [15] since biocompatible [16,17].

The objective of this work is to present a systematic investigation of the calcinations, milling and washing conditions on the final particle size distribution, specific surface area and on the physical–chemical surface properties of a Brazilian bovine bone ash, and to discuss the influence of the results on the processing of the bone china.

2. Experimental

2.1. Material preparation

Bovine bones were heat-treated with steam at 100 °C and 1 atm to remove most meat and blood content. The cleaned bone was dried at 100 °C and heat-treated at 700, 800, 900, and 1000 °C, using a 2 °C min^{-1} ramp and 1 h isotherm. In all cases, air was fluxed inside the furnace to guarantee complete organic burning. The bones treated at the different temperatures were crushed using porcelain mortar and ball milled with distilled water in a porcelain mill containing porcelain elements for 24 h. The milled bones were filtered and abundantly washed with distilled water.

The bone ash was ball milled while simultaneously washed in distillated water or acid solutions at different pH according to dynamic electrophoretic mobility measurements. pH adjustments were carried out using HNO_3 or NH_4OH solutions (2N) provided by Synth, Brazil, in analytical grade.

2.2. Characterization

The bone powders were characterized by scanning electron microscopy (SEM) using a FEI, QUANTA 600 FEG, with an acceleration tension of 10 kV, after a Pt/Au surface coating. The crystalline phase structures of the powders were studied by X-ray diffraction (XRD), using Bruker AXS Model D8 Advance, operating with Cu-Kα radiation, with 0.02° step and 5 s of exposition time per step. The isoelectric point of the powders was determined by measuring the dynamic electrophoretic mobility (MATEC ESA-9800) of an aqueous suspension of each powder (1 vol.%) during titration with HNO_3 (2N solution) in the pH range from 11 to 3. The specific surface area, SSA, of the calcined powders was determined from N_2 adsorption experiments using the BET method; the measurements were performed with Micromeritics Gemini III 2375 equipment; samples were pre-heated at 350 °C during 12 h under vacuum to decrease adsorbed water molecules. Infrared spectroscopy of the powders with a diffuse reflectance apparatus (DRIFT, Magna 560 Nicolet) was also carried out; for the DRIFT measurements, the powders were dried for 6 h at 70 °C and the measurements were carried out in the 400–4000 cm^{-1} wave number range, using 128 scans and step of 0.04 cm^{-1}. The particle size distributions were obtained by laser diffraction/scattering using a Mastersizer 2000 - Malvern Instruments in isopropyl alcohol media. All bone ash dispersion was ultrasonicated for 1 min before each measurement. The densities were measured with an AccuPyc 1330 Helium Pycnometer (Micromeritics Instrument Corporation, Norcross, GA) with the samples treated into a vacuum stove at 250 °C for a few hours.

3. Results and discussion

3.1. Bone ash calcination temperature and milling

Fig. 1 shows the particle size distributions obtained by low angle laser scattering of the bones heat-treated at different temperatures under air before grinding or washing. Two families of particle sizes are mainly observed, one at 4 μm and another at 400 μm. In addition to the small differences due to manual grinding process variations, the figure shows that the relative amounts of these families slightly change with calcination temperature, such that for 900 and 1000 °C samples, a larger amount of the 400 μm family is detected when compared to 700 and 800 °C. This can be attributed to particles coarsening or agglomeration that is activated by temperature. Fig. 2 shows the particle sizes of the same samples after ball milling for 24 h in water. When comparing to Fig. 1, one may note that the family at 400 μm disappears for all samples, while the families at 4 μm and a small one at 0.3 μm increase. This suggests that the ball milling process helps to break agglomerates, freeing the particles and making them suitable for the subsequent processing.

Table 1 shows the SSA of the powders after ball milling. The results show a decreasing SSA with increasing calcination

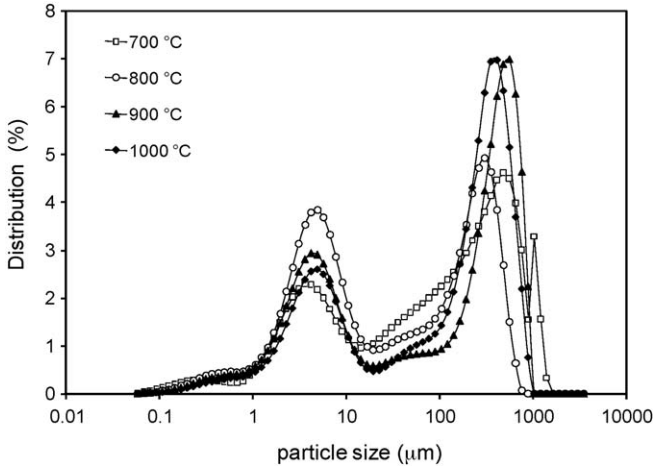

Fig. 1. Particle size distribution of bovine bone calcined at different temperatures before grinding and washing.

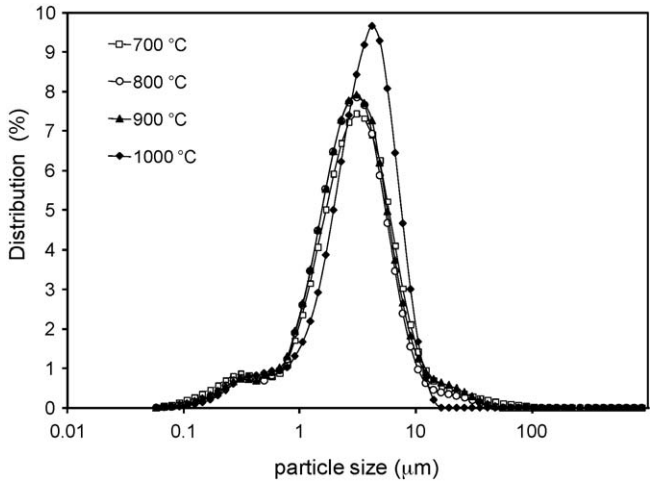

Fig. 2. Particle size distribution of bovine bone calcined at different temperatures after milling and washing.

temperature, which is consistent with a coarsening process that can be evidenced by the median particle size evolution calculated from the SSA and the densities measured by pycnometry (also shown in Table 1) using a spherical approach – D_{SSA}. Table 1 shows that D_{SSA} slightly grows from 700 to 900 °C, and shows a remarkable increase from 900 to 1000 °C. Comparing the estimated particle sizes with those measured by laser scattering, one may note that all D_{SSA} are in the range of the small family at 0.3 μm. This could indicate two possibilities: (1) the diameters calculated based on SSA are unreal due to particle morphology or (2) the particles are agglomerated even after milling, leading to larger results by laser scattering.

Table 1
Specific surface area and density of bone calcined at different temperatures and the calculated mean particle size, D_{SSA}.

Calcination temperature (°C)	SSA (m^2/g)	Density (g/cm^3)	D_{SSA} (μm)
700	5.09	2.91	0.40
800	4.57	2.51	0.52
900	4.41	2.52	0.54
1000	2.56	2.52	0.93

Fig. 3 shows the SEM of the powders after milling. One may observe that the isolated particles are reasonably isotropic and their sizes confirm that D_{SSA} indeed represents an average particle size. In particular, Fig. 3d shows that the particles heat-treated at 1000 °C are considerably larger than the others, as suggested by D_{SSA}. Hence, we may conclude that the laser scattering family at 4 μm detected for the milled powders might be attributed to agglomerates, since the particles sizes based on SEM are mostly smaller than 1 μm for all treatment temperatures. However, the particles size distribution is homogeneous, based on the presented SEM, and suitable for application in ceramic processing for all the studied temperatures.

The particle size distribution of bones have already been presented by Cooper [3] for bones heat-treated at 800, 1000, and 1200 °C. In that case, the mean particle sizes obtained by sedimentation techniques were 0.5, 1.0, and 2.0 μm, respectively. Comparing to the presented data on Table 1, the diameters for 800 °C treatments are consistent, but that for 1000 °C differs by a factor two. However, not enough details on the bone heat-treatment and milling processing were described by Cooper [3] and an objective confrontation of the results is not possible.

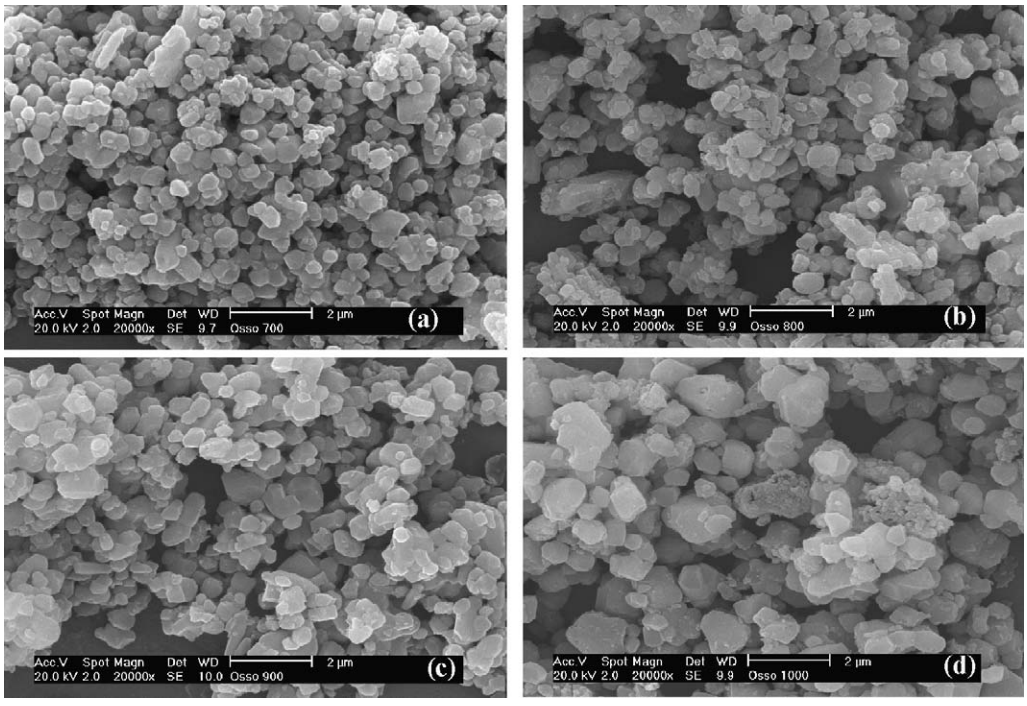

Fig. 3. SEM of milled and washed bone particles calcined at different temperatures: (a) 700 °C, (b) 800 °C, (c) 900 °C and (d) 1000 °C.

Table 2
XRF chemical analysis of bone calcined at different temperatures before and after milling and washing (MW).

Oxide (%)	Sample							
	700 °C	800 °C	900 °C	1000 °C	700 °C (MW)	800 °C (MW)	900 °C (MW)	1000 °C (MW)
CaO	**55.3**	**55.3**	**55.3**	**55.6**	**54.6**	**54.6**	**55.0**	**55.0**
P_2O_5	41.9	42.0	42.1	41.7	42.7	42.8	41.9	42.6
Na_2O	**1.33**	**1.25**	**1.10**	**1.11**	**1.10**	**0.97**	**1.20**	**0.74**
MgO	1.11	1.11	1.12	1.13	1.11	1.12	1.34	1.12
Al_2O_3	0.01	<<	n.i.	n.i.	0.19	0.24	0.18	0.21
SiO_2	0.02	0.01	n.i.	n.i.	0.04	0.06	0.04	0.02
SO_3	0.13	0.16	0.18	0.18	0.09	0.10	0.16	0.18
Cl	0.10	0.13	0.07	0.06	0.07	0.07	0.06	0.06
K_2O	**0.40**	**0.03**	**0.02**	**0.02**	**0.02**	**0.02**	**0.01**	**n.i.**
ZnO	0.02	0.02	0.02	0.02	0.02	0.02	0.01	0.02
SrO	0.06	0.06	0.06	0.07	0.06	0.06	0.06	0.06
BaO	0.02	<<	n.i.	0.10	0.03	0.03	0.04	n.i.
Fe_2O_3	0.01	<<	<<	0.01	<<	<<	<<	<<

<<, traces; n.i., non-identified.

3.2. Bone ash chemical and structural properties

Most of the chemical composition of bone ashes is hydroxyapatite. However, as a natural material, it is usual to find traces of a number of mixed oxides as minor phases or as solid solution [3]. Table 2 shows the chemical composition analysis obtained by XRF of the calcined bone ashes before and after milling and washing. From the table, it is observed that the chemical composition of the powders submitted to the same process (i.e. washing with water and milling or no-washing and no-milling) are rather similar, regardless the calcination temperature, suggesting that decompositions and reactions are not observed in the studied temperature range (as reinforced by XRD commented below). The average chemical composition of the bones treated at different temperatures before and after milling and washing are also similar and only slight changes can be observed. After milling in distilled water with porcelain milling elements, an increase in Al and Si content, and a decrease on Na, Ca, and K contents are observed for all calcination temperatures. The increase of Al and Si has been previously reported to be related to porcelain milling contaminations [3]. The decrease in the Na, Ca, and K content can be attributed to the dissolution of soluble species. Table 2 also shows a very small amount of iron oxides in the bones before and after milling. This indicates the high efficiency of meat and blood removal in the beginning of the process, and reinforces the applicability of this raw material to obtain optimal visual properties of porcelains.

Fig. 4 shows the XRD patterns of the bone ashes heat-treated at different temperatures before washing with water and milling. Fig. 4 indicates the presence of hydroxyapatite (JCPDS #240033). For the samples treated at all temperatures and unwashed, a small amount of another crystalline phase was observed as pointed in the graph. The phase was associated to a soluble phase, possibly a carbonate of soluble salts [JCPDS #150100 – $(Ca,Mg,Na,H_3)_5(P,C)_3O_{12}(OH,F,Cl)$]. Worthy to note that after milling and washing with water, the carbonate related peaks are no longer detected as pointed by the absence of the peak at ~37.4°. The reduction of calcium and sodium amount evidenced by XRF analysis (Table 2) after washing could be associated to the solubility of calcium and sodium compounds. However, the XRD technique has limitations in the identification of low level or surface contaminants. In fact, surface analysis shown below indicates that the pure water washing was not enough to remove the total carbonate compound from the bone ashes even after calcination at 1000 °C and further water washing. This carbonate is supposed to be located on the surface of the powders and will strongly affect further processing of the ash if not removed by the correct procedure.

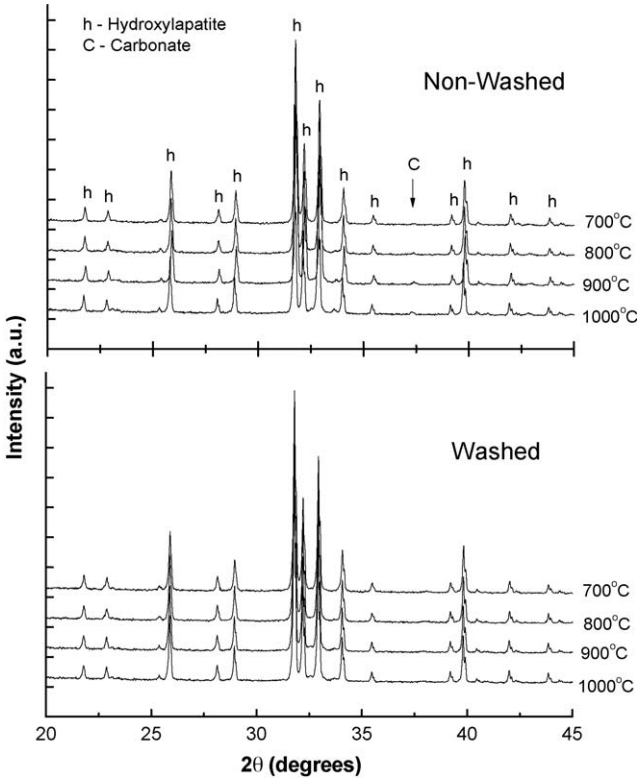

Fig. 4. XRD of bone calcined at 700–1000 °C before milling and washing and after washing with H_2O.

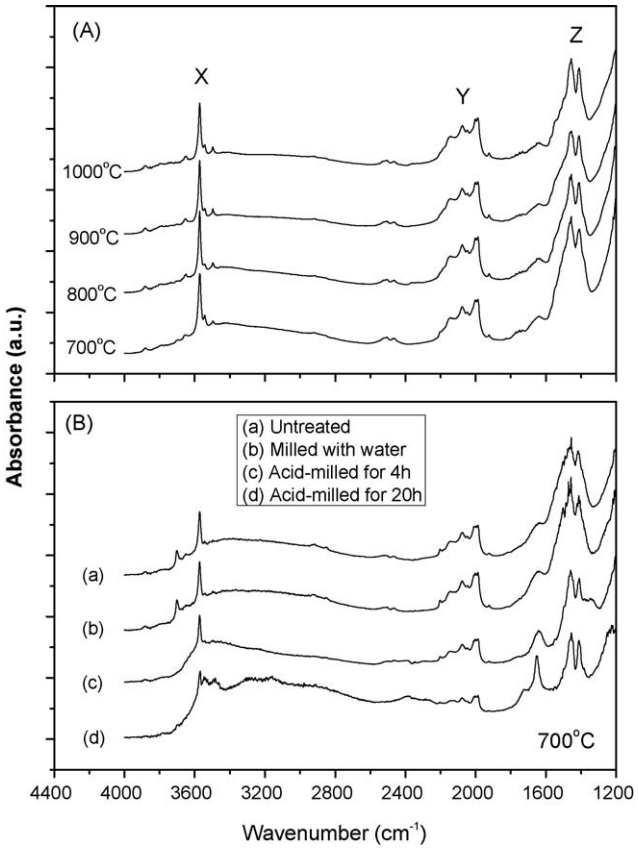

Fig. 5. FTIR-DRIFT spectra of (a) the calcined bovine bone at 700, 800, 900 and 1000 °C with air injection in the oven atmosphere before grinding and washing. (b) Bone ash powders calcined at 700 °C and washed in different conditions as pointed in the graph.

3.3. Bone ash surface analysis

Surface physical–chemical properties of oxides are extremely important to choose the best dispersant agent and obtaining high stability of ceramic suspensions for subsequent forming by, for example, slip casting. Bone china dispersions are reported to be usually unstable and a relation between the aging time and dispersion stability was observed [3]. The poor dispersion stability is attributed to the bone ash surface reactions, but the specific reasons for these behaviors are not completely known. A reported explanation is the formation of –CNO and –CN groups on the surface of the particles due to incomplete burning of the organic materials [3]. These groups could be changed as a consequence of interactions with the solvent. To avoid this problem, it is common to treat the bone ashes at temperatures higher than 1000 °C to assure total organic materials burning. However, a study of the surface evolution as a function of the thermal treatment is not reported to the best of our knowledge.

Fig. 5a shows the FTIR–DRIFT analysis of bones after calcination and before milling. DRIFT is a technique that allows a higher contribution of the surface chemistry to the infrared spectrum, such that it can provide important insights about the surface chemistry [18,19]. FTIR absorption bands of synthetic hydroxyapatite, $Ca_5(PO_4)_3(OH)$ were only observed in two ranges: 1150–963 cm^{-1} for the $\nu 3$ mode and 655–548 cm^{-1} corresponding to $\nu 4$ absorption of the phosphate groups [20]. In our work, the same absorption bands were observed for all spectra. However, three other IR band sets could be assigned as indicated in Fig. 5: X, 3571.6, 3550.4 and 3498.3 cm^{-1}; Y, 2154.1, 2080.8, 2005.6 and 1994.1 cm^{-1}; and Z, 1459.9 and 1415.5 cm^{-1}. In previous work [3], the Y set was attributed from surface cyanide group substituted for –OH in the apatite lattice and the Z due to surface carbonates species. The X set is generally attributed to adsorbed –OH stretching [19,20].

A recent work concerning *in situ* FTIR of CO and CO_2 adsorption on CaO and phosphated CaO (P-CaO) surfaces reports a strong absorption at 2173–2163 cm^{-1} due to CO adsorption on P-CaO surface at 85 K [20]. FTIR band set Y could be associated to CO_2 adsorption on the Ca^{2+} surface sites [21]. Freshly CaO powder exposed to CO_2 presents a broad structureless band between 1560 and 1360 cm^{-1} and a shoulder at 1630 cm^{-1}. Philipp and Fujimoto [21] attributed a weak band at 2213 cm^{-1} also to CO_2 adsorption. It was proposed that some of adsorbed CO_2 could be transformed into bicarbonates species on the CaO surface by reaction with adsorbed water. The adsorbed groups showed a high chemical stability and temperatures as high as 1000 °C and were not sufficient to remove the species from the bone ash surface. From this, one could suggest that bone calcination sub-products could be adsorbed on the surfaces and the dispersions stability would be related to modifications of these species during dispersion aging. Considering the detailed work of CO and CO_2 adsorption on phosphated CaO, we could suppose that only carbonated species, and not the cyanide groups, are adsorbed on the bone ash surface, since the bands find in the Zaki work [20] are very similar to those in Fig. 5. A detailed study about the relationship of adsorbed species on bone ash and dispersion stability will be proposed in a near future.

To evaluate the effect of washing in the surface chemistry, Fig. 5b shows the FTIR of the bone powders calcined at 700 °C and washed by ball milling with pure water. Differently from what was observed in the XRD data, the washing procedure (washed with water) seems not to be effective in changing the surface composition of the powder, and all bands assigned as X, Y, and Z are very similar before and after washing. This suggests that the carbonate is concentrated on the surface and cannot be detected by XRD.

To remove the carbonate from the surface that was probably formed due to a combination of carbon burning from organic materials with the present ions as Na and Ca, a titration of the powder in suspension as a function of dynamic mobility was carried out to study possible surface reactions. Fig. 6 shows the electrokinetic dynamic mobility of bone ashes treated at the different temperatures in aqueous suspension as a function of pH. In general, the suspension of non-washed powders presented a similar behavior with a small modification in the isoelectric points, IEP, that varied from 9.5 to 10.5. The small difference can be attributed to the heterogeneities of chemical composition and specific surface area of the samples. Even so, the data confirms that the surface chemistry of the powders is almost similar. Indeed all surfaces present an anomalous

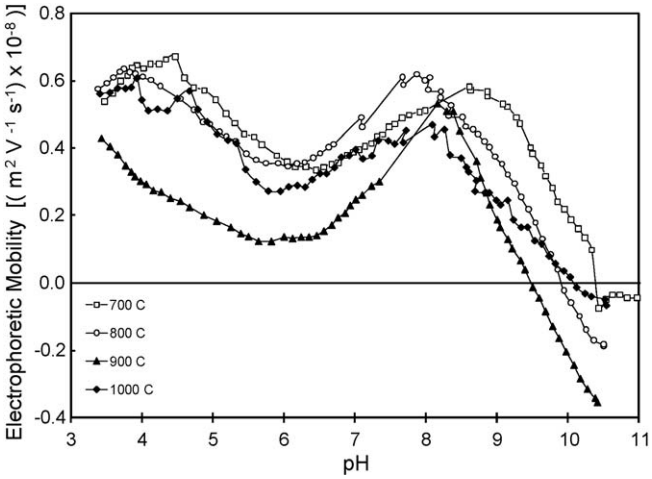

Fig. 6. Electrokinetic dynamic mobility of bone ash versus pH of bovine bone calcined at 700, 800, 900 and 1000 °C.

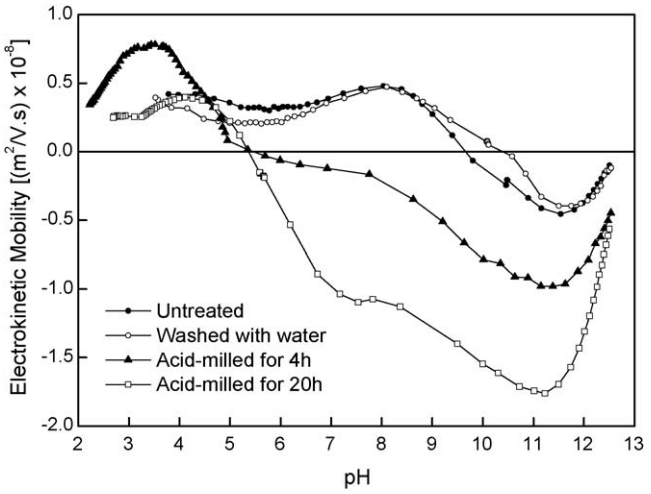

Fig. 7. Electrokinetic dynamic mobility of bone ash dispersion versus pH of bovine bone calcined at 700 °C and washed at different conditions as indicated in the graph.

phenomenon in the pH ranging from 8 to 6, where the dynamic mobility for all samples decreased with decreasing pH. Usually, when decreasing the pH of an aqueous oxide suspension, the surface is simply reacted with H_3O^+ groups, that is specifically adsorbed, and is positively charged. Therefore, an increase in the mobility is usually observed. The anomalous behavior can here therefore be attributed to a reaction between the acid solution and the adsorbed species. This suggests that, at acid pH, the surface is being ''cleaned'' and the adsorbed carbonates would be solubilized.

To assure that the acid was indeed removing adsorbed species from the surface, a new procedure of bone ash washing was proposed. The powders were ball milled for two different times (4 and 20 h) in suspensions with pH set to 1 by adding HNO_3. After that the powders were washed with water to remove residual HNO_3. Fig. 5b shows the FTIR spectra of the powders washed following the new procedure at pH 1. The infrared region attributed to –OH stretching was changed such that the pronounced peak at 3700 cm^{-1} vanished and two new peaks appeared at about 3500 cm^{-1}. This suggests that the chemical composition of the bone ash surface was modified and new hydroxyl groups appeared as a consequence. For the sample treated for only 4 h, those last hydroxyl bands were less pronounced meaning the adsorbed agents were still attached to the hydroxyl groups. These modifications were accomplished to slight changes in the 1450 cm^{-1} region (Z group). The non-vanishing of the Z group, attributed to carbonate related bonds, can be interpreted as (1) the washing was not complete, or (2) these bands could be related to other groups in addition (e.g. hydroxyls). Future studies on the washing process will be presented soon.

The surface cleanness after the proposed acid washing procedure is shown in Fig. 7 for powders treated at 700 °C. The dynamic mobility of the particles after washing is observed to be different from those obtained for the non-washed powders. In fact, the curve for the clean powder presented an IEP of about 5.6 and a regular curve that can be easily interpreted in terms of hydroxyl surface groups interacting with specific adsorption of H_3O^+ and OH^-. Moreover, by comparing the powder acid washed by 4 and 20 h, one may conclude that the surface was progressively cleaned as shown in the FTIR data.

The electrical conductivity of the bone ash dispersions (Fig. 8) presents an anomalous increase in the 6–8 pH range for both untreated and water washed powders suspensions. An atypical dynamic mobility behavior was verified in the same pH range (Fig. 7) and could be associated to the solubilization of the adsorbed carbonate during dynamic mobility measurements. After acid washing (for both 4 and 20 h), the anomalous increase of conductivity was not detected (Fig. 8), reinforcing that the bone ash surface was cleaned during the washing process. The surface chemistry change of the particles could be also associated to the modification of particle size during milling by the creation of new surfaces. The analysis of particle size distribution during milling and washing process did not show modification in the particle size (Fig. 9) as well as in the specific surface area (Table 3), reinforcing that all electrokinetic mobility changes were associated to the surface chemistry during acid washing and milling processes.

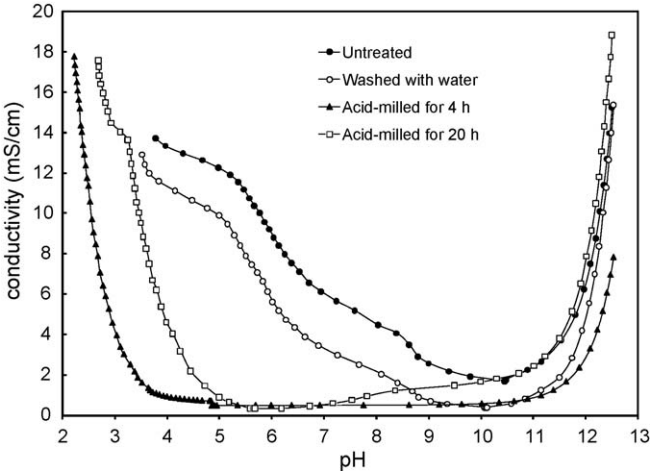

Fig. 8. Electrical conductivity of bone ash dispersion versus pH of bovine bone calcined at 700 °C and washed at different conditions as indicated in the graph.

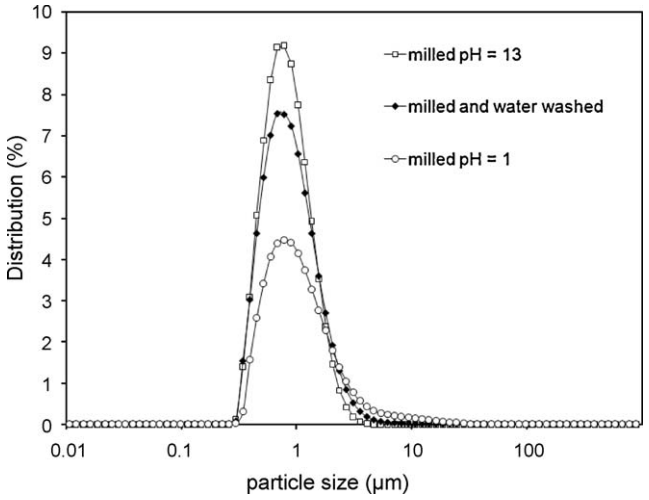

Fig. 9. Particle size distribution of bovine bone calcined at 700 °C and milled in water, acid solution (pH 1) and basic solution (pH 13).

Table 3
Specific surface area of bovine bone ash treated by different process.

Process	SSA (m^2/g)
Milled pH 13	6.89
Milled and water washed	6.09
Milled pH 1	6.90

4. Conclusions

Bone ashes properties were studied by DRIFT, XRD, XRF and electrophoretic dynamic mobility as a function of heat treatment and washing procedure. It is observed that the calcination temperatures (varied from 700 to 1000 °C) did not significantly influence the composition of the bone ash, but just lead to an increasing particle size. However, water washing of the bone ashes treated at the different temperature decreased the amount of carbonate such that it could not be detected by XRD.

The pure water cleaning process showed however inefficient when observing the FTIR spectra of the powders. In that case the surface still showed a high concentration of carbonate related species. After a study of dynamic mobility as a function of pH, it was determined an optimal condition for removing adsorbed carbonate from the bone ash particles surface. This was basically a ball milling using acid (HNO_3) to achieve pH 1. This acid washing removed the adsorbed species such that the regular dynamic mobility curve as a function of pH could be obtained and an IEP of 5.3 was measured for bone ash.

Acknowledgements

The authors would like to thank the financial support from FAPESP (Desenvolvimento do Processo Nacional para a Fabricação de Porcelana de Ossos – Bone China - proc. 03/12721-2), FAPESP Proc. 05/55335-0, CNPq (Projeto MACEPLAS - Edital Universal 01/2002 proc. 475029/2003-8), CAPES and FINEP 5089/06.

References

[1] P. Rado, An Introduction to the Technology of Pottery, second edition, Pergamon Press, Oxford, 1988.
[2] A.J. Forrester, Impact of raw-material changes on bone china manufacture, Br. Ceram. Trans. J. 85 (6) (1986) 180–183.
[3] J.J. Cooper, Bone for bone china, Br. Ceram. Trans. J. 94 (4) (1995) 165–168.
[4] R.G. Hill, K. Webster, C. May, A. Mandal, Microstructural evidence for amorphous phase-separation in bone china, Br. Ceram. Trans. J. 93 (1) (1994) 16–20.
[5] Y. Iqbal, P.F. Messer, W.E. Lee, Microstructural evolution in bone china, Br. Ceram. Trans. J. 99 (5) (2000) 193–199.
[6] Y. Iqbal, P.F. Messer, W.E. Lee, Non-equilibrium microstructure of bone china, Br. Ceram. Trans. J. 99 (3) (2000) 110–116.
[7] P.D.S.S. Pierre, Constitution of bone china. 3. High-temperature phase equilibrium studies in the system tricalcium phosphate–anorthite–silica, J. Am. Ceram. Soc. 39 (4) (1956) 147–150.
[8] A. Kara, R. Stevens, Characterisation of biscuit fired bone china body microstructure. Part I. XRD and SEM of crystalline phases, J. Eur. Ceram. Soc. 22 (5) (2002) 731–736.
[9] A. Kara, R. Stevens, Characterisation of biscuit fired bone china body microstructure. Part II. Transmission electron microscopy (TEM) of glassy matrix, J. Eur. Ceram. Soc. 22 (5) (2002) 737–743.
[10] A. Kara, R. Stevens, Interactions between an ABS type leadless glaze and a biscuit fired bone china body during glost firing. Part I. Preparation of experimental phases, J. Eur. Ceram. Soc. 22 (7) (2002) 1095–1102.
[11] A. Kara, R. Stevens, Interactions between an ABS type leadless glaze and a biscuit fired bone china body during glost firing. Part II. Investigation of interactions, J. Eur. Ceram. Soc. 22 (7) (2002) 1103–1112.
[12] T. Ichiko, A consideration about the glazing to the bone china, J. Ceram. Soc. Jpn. 102 (5) (1994) 471–475.
[13] A. Kara, R. Stevens, Interactions between a leadless glaze and a biscuit fired bone china body during glost firing. Part III. Effect of glassy matrix phase, J. Eur. Ceram. Soc. 23 (10) (2003) 1617–1628.
[14] P.D.S.S. Pierre, Constitution of bone china. 2. Reactions in bone china bodies, J. Am. Ceram. Soc. 38 (6) (1955) 217–222.
[15] C.Y. Ooi, M. Hamdi, S. Ramesh, Properties of hydroxyapatite produced by annealing of bovine bone, Ceram. Int. 33 (7) (2007) 1171–1177.
[16] R.V. Silva, J.A. Camilli, C.A. Bertran, N.H. Moreira, The use of hydroxyapatite and autogeneous cancellous bone grafts to repair bone defects in rats, Int. J. Oral Maxillofac. Surg. 10 (2004) 1–7.
[17] P.G. Whang, J.C. Wand, Bone graft substitutes for spinal fusion, Spine J. 3 (2003) 155–165.
[18] P. Hidalgo, R.H.R. Castro, A.C.V. Coelho, D. Gouvea, Surface segregation and consequent SO_2 sensor response in SnO_2–NiO, Chem. Mater. 17 (16) (2005) 4149–4153.
[19] G.J. Pereira, R.H.R. Castro, P. Hidalgo, D. Gouvea, Surface segregation of additives on SnO_2 based powders and their relationship with macroscopic properties, Appl. Surf. Sci. 195 (1–4) (2002) 277–283.
[20] M.I. Zaki, H. Knozinger, B. Tesche, G.A.H. Mekhemer, Influence of phosphonation and phosphation on surface acid–base and morphological properties of CaO as investigated by in situ FTIR spectroscopy and electron microscopy, J. Colloid Interface Sci. 303 (1) (2006) 9–17.
[21] R. Philipp, K. Fujimoto, FTIR spectroscopic study of CO_2 adsorption/desorption on MgO/CaO catalysts, J. Phys. Chem. 96 (22) (1992) 9035–9038.